CHEMISTRY OF MATERIALS

Article

pubs.acs.org/cm

Solid-Solution Li Intercalation as a Function of Cation Order/Disorder in the High-Voltage $Li_xNi_{0.5}Mn_{1.5}O_4$ Spinel

Eunseok Lee* and Kristin A. Persson

Environmental Energy Technologies Division, Lawrence Berkeley National Laboratory, Berkeley, California 94720, United States

Supporting Information

ABSTRACT: Many Li-ion cathode materials transform via two-phase reactions, which can lead to long-term structural damage and limited cyclability. To elucidate the coupling between favorable solid-solution Li intercalation and the underlying cation ordering, we take the high-voltage spinel, $Li_xNi_{0.5}Mn_{1.5}O_4$ ($0 \leq x \leq 1$), as a case example. Through grand canonical Monte Carlo (MC) simulations based on the ab initio cluster expansion model, we show a striking dependence between the solid-solution phase domain and the Ni−Mn cation ordering. The perfectly ordered $Li_xNi_{0.5}Mn_{1.5}O_4$ spinel resists solid solution until very high temperatures, but introducing various degrees of Ni−Mn cation disorder results in a dramatic increase in stability for a single-phase reaction, particularly at high Li contents. This opens up the possibility of designing single-phase reaction materials via targeted cation ordering, and to this end, we show that a uniformly distributed cation high-voltage spinel has access to solid solution throughout the entire Li composition range at room temperature.

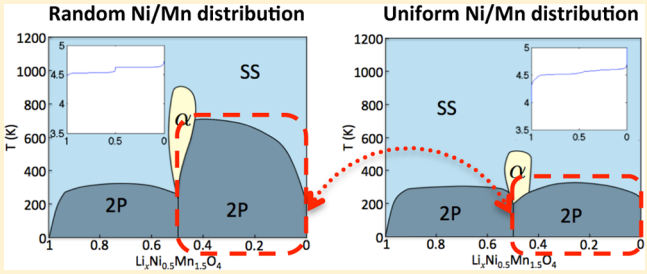

KEYWORDS: *Ni−Mn spinel, rate capability, phase diagram, solid-solution, first-principles calculation*

INTRODUCTION

Several well-known Li-ion battery electrode materials are known to transform according to wide-range two-phase reaction mechanisms.[1−8] A two-phase reaction process and the accompanying mechanical strain due to coexisting phases with significantly different crystallographic dimensions within the same particle are likely to cause irreversible long-term structural damage to the material during cycling, thus limiting the lifetime of the battery. The nucleation and growth processes in a two-phase reaction will add extra kinetic barriers to the lithiation and delithiation. Furthermore, the sloping voltage profile associated with a single-phase reaction presents easier and cheaper monitoring of the state of charge of the battery, as compared to a flat voltage curve associated with a two-phase reaction. Thus, it is desirable to design or modify cathode materials to enhance the accessibility of the solid-solution phase domain and transform via a single-phase reaction, without sacrificing other favorable properties.

Previous work has shown promise in this direction through defect chemistry, substitutions, and size-control, especially for $LiFePO_4$.[1,7,9−12] Delacourt et al.[9] demonstrated the existence of complete single-phase Li_xFePO_4 solid solution at high temperatures (350 °C) as opposed to the classical RT two-phase description. Gibot et al.[12] showed that a substantial concentration (20%) of Li/Fe antisite defects and vacancies together with nanosizing (40 nm) in $LiFePO_4$ induces solid solution even at RT. However, the exact reaction mechanism of $LiFePO_4$ remains in debate as Malik et al.[1] suggested that the material preferentially transforms through rapid short-range order or solid-solution nonequilibrium reactions, and then relaxes to the ground-state two-phase state. In other cathode materials, defect substitutions in the Mn spinel (see, e.g., Hong et al.[10] and references therein) and Ti substitutions for Fe in the Nasicon $LiTi_2(PO_4)_3$ have been shown to increase the single-phase domain behavior.[11] There is evidence of controlling the phase behavior of cathode materials by manipulating the particle size alone. Wagemaker et al.[7] showed that very small (7 nm) particle anatase TiO_2 can host up to 0.21 Li/Ti as compared to 0.03 Li/Ti for microcrystalline particles, which is believed to be associated with the extension of the solid-solution phase domain due to the nanosizing. However, the hitherto applied approaches may present other drawbacks for the battery material performance. Defects[12] or substitutions with inactive cations[13,14] will lower the inherent capacity of the material, and nanosizing[15,16] generally leads to increased reactivity with the electrolyte as well as lower energy density of the composite electrode. The question arises whether we can design electrode materials for single-phase reaction using the inherent chemistry of the system while preserving the overall qualities of the material.

In this paper, we use first-principles grand canonical MC simulations to establish and invert the relation between cation ordering and the existence of RT accessible solid-solution transformation paths as a function of Li content and temperature. We choose to demonstrate the approach on a promising high-energy density cathode material: the high-

Received: May 3, 2013
Revised: June 29, 2013
Published: July 1, 2013

voltage spinel, $LiNi_{0.5}Mn_{1.5}O_4$, which exhibits fair capacity (≈150 mAh/g) and rate capability.[17,18] The high-voltage spinel is a suitable candidate for this study as it displays a variety of equilibrium Li-vacancy two-phase transformation processes[8] depending on the cation ordering and we can study several cases within the same structural and chemical system. By manipulating the cation arrangement, we find a striking dependence between the preferred Li reaction mechanism and the inherent cation ordering, which is corroborated by existing experiments. Finally, we utilize the relationship to identify a cation arrangement for achieving solid-solution behavior at RT for all Li compositions.

COMPUTATIONAL MODEL AND METHODOLOGY

Depending on the synthesis procedure, the $Li_xNi_{0.5}Mn_{1.5}O_4$ ($0 \le x \le 1$) system exhibits two overall cation arrangements, one of which is illustrated in Figure 1.[18,19] In this perfectly ordered arrangement, the Ni and Mn ions are located at 4*b* and 12*d* sites, respectively. The 8*a* sites can be occupied by Li ions or remain vacant (labeled "VA" hereafter) depending on the state-of-charge (see Figure 1). The ionic configuration of this unit cell corresponds to the $P4_332$ space group. In the cation-disordered material, the Ni and Mn ions are distributed randomly on any of the 4*b* and 12*d* sites and the corresponding ionic configuration belongs to the $Fd\bar{3}m$ space group. Within the disordered material, we find it instructive to study local cation arrangements and their contribution to the properties of the material. Specificially, within any random cation ordering, the local cation arrangement that has the highest number of permutations, that is, occupies the highest degree of the configuration phase space, is a uniform distribution of the Ni and Mn ions in which the Ni ions are uniformly distributed on the 4*b* and 12*d* sites, with no distinction between them, forming an fcc sublattice. The atomic structure of this uniform distribution is illustrated in the Supporting Information. Although several research teams infer small amounts of oxygen deficiency in the disordered material from the oxygen gas evolution during synthesis and the Mn^{3+} content,[20−23] the observed phenomena can also be explained by the formation of impurity phases, such as rocksalt. Indeed, a recent neutron diffraction measurement by Cabana et al. finds no evidence of oxygen vacancies and suggests no correlation between the oxygen deficiency and the Mn^{3+} formation.[24] In this work, no oxygen vacancies are included as we aim to deconvolute the influence of impurity phases and ions from the intrinsic behavior of the material and study solid solution as a function of cation ordering in a general perspective.

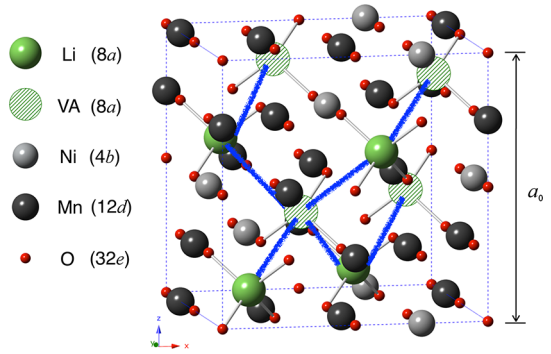

Figure 1. Illustration of the ordered $Li_{0.5}Ni_{0.5}Mn_{1.5}O_4$ ($P4_332$ space group). The tetrahedral (8*a*) and octahedral (4*b* and 12*d*) sites as well as the lattice parameter a_0 are indicated. Blue lines indicate the preferred Li/VA ordering following a zigzag pattern.[8]

The $Li_xNi_{0.5}Mn_{1.5}O_4$ system is described using a cluster expansion based on a total of 251 density functional theory data sets mapping out the connection between the Li/VA and Ni/Mn interactions.[8] Using this converged and bench marked set of interactions, we perform grand canonical MC simulations by perturbing the Li/VA arrangement for a range of fixed Ni/Mn arrangements. We excluded possible Li insertion/extraction from octahedral sites for two reasons: Li is less stable at the octahedral site, which—if utilized in the redox process—typically results in a significant voltage drop to lower than 3 V.[25−27] This lower-voltage capacity is also usually accompanied by a severe phase transformation and rapid capacity fade.[25] Most Li-ion battery applications limit the useful voltage range to >2.7 V, and hence, we excluded octahedral Li insertion/extraction from our investigation.

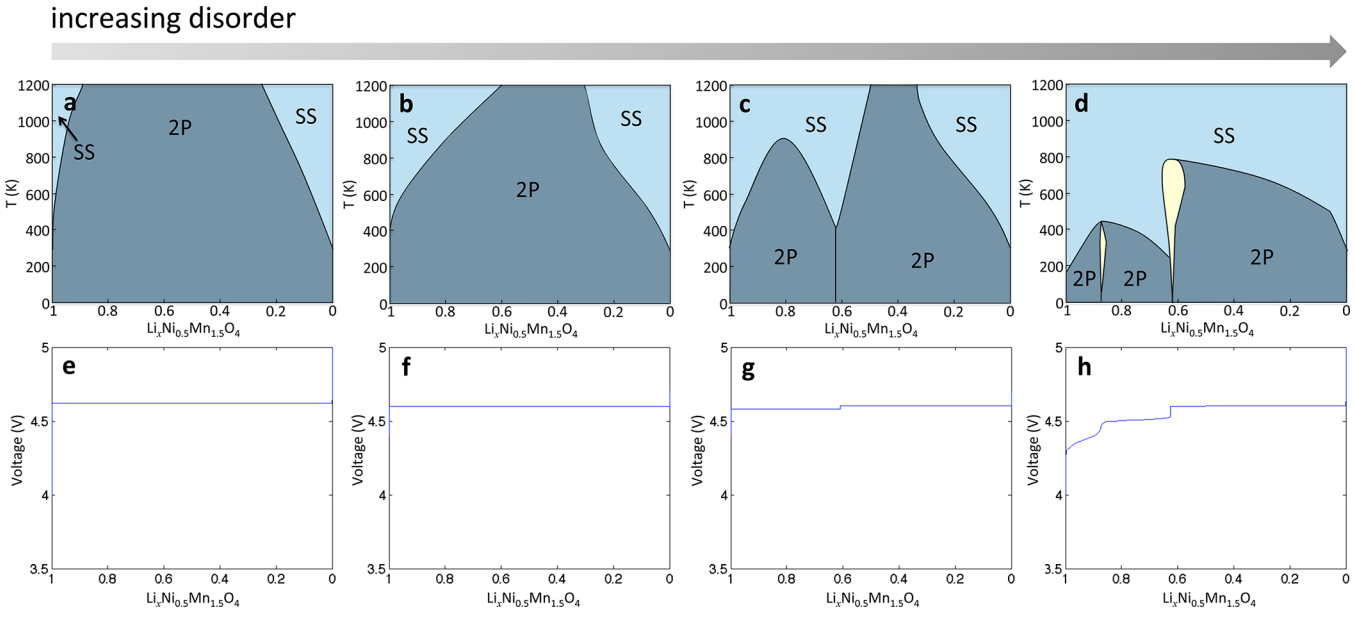

Figure 2. Phase diagram in $T-x$ space for the (a) ordered, (b) 1/32-deviated, (c) 1/16-deviated, and (d) 1/4-deviated arrangements. "1/*n*-deviated" indicates that one Ni ion per *n* Ni ions is deviated from the perfectly ordered arrangement (e.g., exchanged site with a Mn ion). This model is not intended to capture true disorder in a large sample, but to illustrate the effect of local deviations from perfect cation ordering on the phase behavior. "SS" and "2P" indicate solid-solution and two-phase reaction regions, respectively. Panels (e)−(h) are the voltage profiles calculated at 300 K corresponding to (a)−(d), respectively.

dx.doi.org/10.1021/cm4014738 | *Chem. Mater.* 2013, 25, 2885−2889

During the grand canonical MC simulation, the grand potential Ω is obtained: $\Omega = E - \mu_{Li}x_{Li}$, where E is the energy of system, μ_{Li} is the Li chemical potential, and x_{Li} is the Li content. Within the formalism of a grand canonical ensemble, the Li chemical potential μ_{Li} is fixed but x_{Li} is allowed to change. The free energy calculation, *in principle*, requires a prediction of the total energy as a function of all possible ionic configurations, which is intractable. Instead, we first calculate the free energy difference by thermodynamic integration of the grand potential and then calculate the free energy with respect to a reference free energy $\Phi(T_0, \mu_0)$: $\Phi(T_0, \mu) = \Phi(T_0, \mu_0) - \int_{\mu 0}^{\mu}\langle N(T_0, \mu)\rangle d\mu$ (along a fixed temperature), or $\Phi(T, \mu_0)/kT = \Phi(T_0, \mu_0)/kT + \int_{T0}^{T}\{\langle E(T, \mu_0)\rangle - \mu\langle N(T, \mu_0)\rangle\}d\beta$ (along a fixed chemical potential). Although the energy and free energy are the same at 0 K, the energy at 0 K is not a good choice for $\Phi(T_0, \mu_0)$ as it causes the infinity to be included in the thermodynamic integration along a fixed chemical potential. Instead, we calculate the free energy at 25 K by a low-temperature expansion and use it for $\Phi(T_0, \mu_0)$. The phase boundary is determined by finding discontinuities in the free energy or the derivative of the free energy with respect to Li chemical potential and temperature. For further details on the methodology, we refer the reader to refs 28 and 29.

One phase diagram is constructed by scanning the Li/VA phase space while changing the chemical potential from −6.8 eV/particle to −6.3 eV/particle at an interval of 0.01 eV/particle and the temperature from 50 to 1200 K at an interval of 50 K. In each case of the chemical potential and temperature, two simulations are performed for two different initial Li contents, fully lithiated and delithiated, to simulate the charge and discharge process, respectively. In each simulation, the total number of MC steps and equilibrium steps are set to 20 million and 1 million, respectively, and the convergence of each simulation is validated by the agreement between the charge and discharge process. From analysis of the free energy as a function of temperature and the chemical potential, we track the phase boundaries in the phase diagram in $T-\mu$ space. The phase diagram in $T-\mu$ space is then converted to the phase diagram in $T-x$ space by finding the Li content corresponding to the chemical potential at the phase boundary. Furthermore, from analysis of the chemical potential versus the Li content, we obtain the voltage profile at finite temperatures.

RESULTS AND DISCUSSION

We obtain the phase diagrams and RT voltage profiles for the perfectly ordered and partially ordered Ni/Mn arrangements using a 2[100] × 2[010] × 2[001] supercell that contains 64 Li, 32 Ni, 96 Mn, and 256 O ions. The resulting $T-x$ phase diagrams are shown in Figure 2. In a perfectly ordered structure, the ground-state two-phase region is stable until T = 1200 K (see Figure 2a), although the range of Li content corresponding to the two-phase region is slightly reduced at the end of charge/discharge at higher temperatures. This persistent two-phase behavior is a direct result of the incompatibility between the preferred zigzag Li/VA ordering (see Figure 1) and the fixed Ni/Mn distribution in the ordered phase, which was explored by the cluster expansion method in our previous work.[8] The corresponding voltage curve at 300 K exhibits a flat profile at around 4.6 V, the magnitude of which is in excellent agreement with experimental observations.[18,19] However, most experimental observations of phase evolution in the $P4_332$ (ordered) $Li_xNi_{0.5}Mn_{1.5}O_4$ as a function of Li content show a two-phase region at low Li contents up to approximately x_{Li} = 0.6–0.7, followed by a predominant solid-solution-like single-phase at high Li contents.[18,30,31] To reconcile these findings with ours, we acknowledge that any real "ordered" $P4_332$ sample exhibits short-range cation disorder, to varying degrees.[8] To investigate how deviations from perfect cation ordering affects the phase behavior, we calculate the phase diagram for several cases of "1/n-deviated" Ni/Mn arrangements, where "1/n-deviated" indicates that one Ni ion per n Ni ions is deviated from the perfectly ordered arrangement. The results are presented in Figure 2b–d. We observe that, as cation disorder is gradually introduced into our model system, the stability of the solid-solution region is enhanced, particularly in the high Li-content region. For the 1/4-deviated arrangement (one Ni out of four is deviated from the perfectly ordered arrangement), the solid solution becomes stable already at 410 K for $x_{Li} > 0.6$ and at 800 K for $0 < x_{Li} < 0.6$. We emphasize that the occurrences of spurious intermediate ordered phases (e.g., $x_{Li} \sim 0.6$ and $x_{Li} \sim 0.9$) in the 1/16- and 1/4-deviated model systems are due to the particular cation ordering in this relatively small supercell and are unlikely to manifest in any realistic sample. Thus, we find that, depending on the degree of ordering of the $P4_332$ sample, the solid-solution region dominates at high Li contents with a preferred two-phase behavior at lower Li contents, which is compatible with experimental results.

To achieve an improved model of the disordered $Fd\bar{3}m$ material, we employ a 28 000 atom large-cell random "toss-of-the-dice" Ni/Mn arrangement, where the occupancies of the 12d and 4b sites are generated by randomly choosing Ni and Mn while keeping the overall composition correct. The only restriction we impose on this randomly generated Ni/Mn cation arrangement is to minimize the number of Ni–Ni nearest TM site neighbors as this pair interaction was found to be highly energetically unfavorable in previous work.[8] Several differently sized supercells (2[100] × 2[010] × 2[001] and 5[100] × 5[010] × 5[001]) were examined to ensure sufficient sample size to suppress the occurrence of spurious ordered phases and to identify the true characteristics of the disordered cation material. The results for the 8[100] × 8[010] × 8[001] supercell are presented in Figure 3. The α-phase at x = 0.5 is

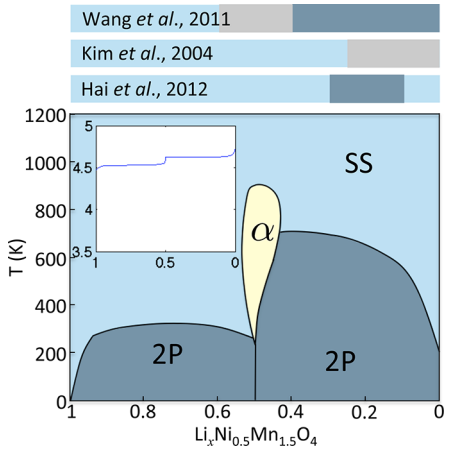

Figure 3. Phase diagram in $T-x$ space for a randomized Ni/Mn arrangement in an 8[100] × 8[010] × 8[001] supercell. The labels "SS" and "2P" indicate solid-solution and two-phase regions, respectively. The colored bars above the graph are reproduced results from three different experimental studies,[18,30,31] where the colors are consistent with the color scheme of the graph and the gray segment indicates unresolved or mixed phase behavior. The inset shows the voltage profile calculated at 300 K.

associated with the compatibility of the preferred Li-VA zigzag ordering with a disordered Ni/Mn arrangement,[8] and manifests in the electrochemical voltage profile as a step of 90 meV at x = 0.5 at RT as compared to a single voltage plateau for the ordered $P4_332$ in Figure 2a. In agreement with our results, numerous experimental works[18,22,30,31] show a distinct voltage step (60–80 meV) at x = 0.5 for the disordered $Fd\bar{3}m$ Ni/Mn

dx.doi.org/10.1021/cm4014738 | Chem. Mater. 2013, 25, 2885–2889

material as compared to the small or negligible one (10−20 meV) for the ordered $P4_332$. Analysis of the evolution of the calculated heat capacity as a function of temperature and Li composition indicates a second-order transition between the α-phase and the solid-solution region: a step discontinuity, rather than a divergent peak, is observed in the heat capacity during the phase transition between the α-phase and the solid-solution region. From Figure 3, we also observe that, for a random cation arrangement in the Ni−Mn spinel, we expect a predominant two-phase reaction at low Li concentrations, a phase transformation at $x = 0.5$ associated with the ordered Li/VA phase, and a single-phase solid solution for $x \geq 0.5$ at RT. For comparison, in Figure 3, we reproduce the reported phase behavior in the cation disordered $Fd\bar{3}m$ material from three different experimental studies.[18,30,31] In agreement with our findings, they show pronounced solid-solution behavior in the cation disordered $Fd\bar{3}m$ material at high Li contents. While the overall trend points to two-phase behavior at lower Li contents and agrees with the calculated predictions, the findings differ somewhat between the different works. We speculate that the differences depend on various degrees of ordering of the samples as well as the measurement techniques.

To design a cation arrangement with an optimally increased solid-solution domain, we use the information we have gathered from the different "ordered" model systems and the large random "disordered" cell. We note that the more "disordered" the cation arrangement is (further away from the ordered arrangement where the Ni and Mn each have their assigned sites 4*b* and 12*d*, respectively), the more stable the solid solution becomes—across the Li composition range. By analyzing the random cation arrangement in the large supercell, we also find that the local Ni/Mn cation distributions indeed locally exhibit a "uniform" environment in ≈20−43% of the sample (the range depending on the assumed size of a "local" domain) due to the high occurrence (entropy) of the "uniform" arrangement within any randomly generated large set. Hence, we postulate that the local cation arrangement corresponding to the highest occurrence within a random sample, that is, a uniform dispersion of Ni and Mn on the 4*b* and 12*d* sites, should result in the largest solid-solution domain. To confirm our prediction, we calculate the phase diagram for a 100% "uniform" arrangement, as shown in Figure 4. Indeed, it manifests the lowest temperature onset of the solid solution, around RT for the entire Li composition range except at $x = 0.5$, where the α-phase occurs. We acknowledge that the as-made disordered $Fd\bar{3}m$ material, just like our large random cell, exhibits many different local cation arrangements that deviate from a perfectly uniform cation distribution. According to our calculations, any such deviation will create tendencies toward two-phase behavior, especially in the low Li content region. Conversely, we predict that attempting to increase the uniformity of the cation ordering by target synthesis conditions and/or inducing cation uniformity by defect design will result in improved access to solid solution throughout the Li composition range. A completely "uniform" arrangement would be considered an ordered state, which is metastable compared to the $P4_332$ phase but likely to be accessible, as shown by its high local occurrence within the disordered material. The corresponding voltage curve at RT for the "uniform" arrangement, shown in the inset of Figure 4, exhibits two smooth (quasi-)plateaus, one between $x_{Li} = 0$ and $x_{Li} = 0.5$ and the other between $x_{Li} = 0.5$ and $x_{Li} = 1$, decreasing gradually with x_{Li} and with an apparent voltage step at $x = 0.5$. In this context, our results in Figures 3 and 4 demonstrate that even stoichiometric $Li_xNi_{0.5}Mn_{1.5}O_4$ spinels with varying degrees of disorder can produce a sloping voltage profile at RT (comparable to the nonstoichiometric $Li_xNi_{0.5}Mn_{1.5}O_{4-\delta}$) due to the solid-solution domain at high Li contents.[19,32]

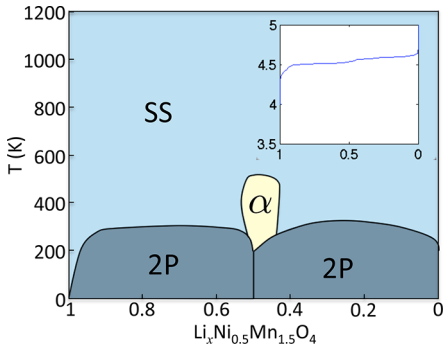

Figure 4. Phase diagram in $T-x$ space for a "uniformly" distributed Ni/Mn arrangement. "SS" and "2P" indicate solid-solution and two-phase regions, respectively. The inset shows the voltage profile calculated at 300 K.

We now discuss the implications of our results for the electrochemical performance of the high-voltage Ni−Mn spinel as a function of its cation ordering. Most studies find that the $Fd\bar{3}m$ material exhibits better rate capability and capacity retention as compared to the ordered $P4_332$ material (see refs 2, 18, 22, and 30 and references therein). In notable contrast, Ma et al.[17] reports very high rates (167C) and excellent capacity retention for micrometer-sized ordered $P4_332$, using a specific electrode and battery design that enhances interparticle contact and Li diffusion rates in the composite electrode. The same electrode design was successfully used for nanometric $LiFePO_4$ to achieve extremely high rates.[33] As both $LiFePO_4$ and $P4_332$ $Li_xNi_{0.5}Mn_{1.5}O_4$ exhibit wide high-strain equilibrium two-phase regions, it is possible that these materials are more reliant on interparticle Li transport in order to achieve high rate capability, which would manifest using the specialized electrode design. Using a conventional electrode design, it has been speculated that the inferior performance seen in electrodes composed of $P4_332$ originates from either one of the following factors or a combination thereof: (i) lower ionic conductivity,[22] (ii) lower electronic conductivity,[23] and (iii) strain associated with two-phase transitions in the ordered material.[18] Our investigation shows that the more ordered the material is, the less likely it is to access any solid-solution region during the lithiation/delithiation cycle, which should negatively impact its cyclability and performance at higher rates. Furthermore, we find that tuning the cation ordering toward a uniform arrangement stabilizes the lowest solid-solution transition temperature across the entire Li composition range. Ready access to solid-solution lithiation reaction mechanisms at RT should correlate with increased rate capability and cyclability, as the nucleation process and the inherent strain associated with sustaining two phases within the same particle can be bypassed.

CONCLUSION

In summary, by investigating the relationship between the inherent Ni/Mn cation disordering and the Li/VA solid-solution phase domain in the high-voltage $Li_xNi_{0.5}Mn_{1.5}O_4$ spinel as a function of temperature and Li content, we find a clear correlation between the underlying transition-metal cation

ordering and the preferred Li intercalation mechanism. A perfectly cation-ordered $Li_xNi_{0.5}Mn_{1.5}O_4$ spinel resists solid solution until very high temperatures, but introducing various degrees of Ni/Mn cation disorder results in a gradual increase in stability for a single-phase reaction, particularly at high Li contents. The cation disordered $Fd\bar{3}m$ material was modeled using a 28 000 atom supercell and a randomized Ni/Mn distribution, which exhibited a predominant two-phase reaction at low Li concentrations, a phase transformation at $x = 0.5$ associated with the ordered Li/VA phase, and a single-phase solid solution for $x \geq 0.5$ at RT. To optimize the domain of the solid-solution reaction, we show that a uniform distribution of Ni/Mn ions has access to the solid-solution domain across the Li composition range at RT, except at $x = 0.5$, where the ordered Li/VA phase occurs. This uniformly "ordered" material exhibits the best access to solid-solution lithiation reaction mechanisms at RT across the Li composition range and should be accessible by target synthesis conditions as a random Ni/Mn distribution already contains a large portion of this cation environment due to its large local contribution to the disordered phase space. Access to solid-solution reaction paths—through either stable or metastable—correlate with increased rate capability and cyclability due to decreased intraparticle strain due to two-phase transitions. A design route for room-temperature solid-solution behavior while preserving the otherwise desirable properties of the material, such as low surface area and inherent capacity, should generate further interest in the battery community as well as in other application areas, such as ionic conductors and solid oxide fuel cells.[34]

■ ASSOCIATED CONTENT

Supporting Information

Illustration of the uniform Ni/Mn distribution in the disordered $LiNi_{0.5}Mn_{1.5}O_4$ sample (PDF). This material is available free of charge via the Internet at http://pubs.acs.org.

■ AUTHOR INFORMATION

Corresponding Author

*E-mail: eunseoklee@lbl.gov.

Notes

The authors declare no competing financial interest.

■ ACKNOWLEDGMENTS

Work at the Lawrence Berkeley National Laboratory was supported by the Assistant Secretary for Energy Efficiency and Renewable Energy, Office of Vehicle Technologies of the U.S. Department of Energy, under Contract No. DE-AC02-05CH11231. Furthermore, this research used resources of the National Energy Research Scientific Computing Center, which is supported by the Office of Science of the U.S. Department of Energy under Contract No. DE-AC02-05CH11231. We are also grateful to Cheonjoong Kim, Jordi Cabana, and Clare Grey for enlightening discussions on the high-voltage spinel.

■ REFERENCES

(1) Malik, R.; Zhou, F.; Ceder, G. *Nat. Mater.* **2011**, *10*, 587−590.
(2) Takahashi, K.; Saitoh, M.; Sano, M.; Fujita, M.; Kifune, K. *J. Electrochem. Soc.* **2004**, *151*, A173−A177.
(3) Takahashi, M.; Ohtsuka, H.; Akuto, K.; Sakurai, Y. *J. Electrochem. Soc.* **2005**, *152*, A899−A904.
(4) Meethong, N.; Huang, H.-Y.; Speakman, S.; Carter, W.; Chiang, Y.-M. *Adv. Funct. Mater.* **2007**, *17*, 1115−1123.
(5) Laffont, L.; Delacourt, C.; Gibot, P.; Wu, M. Y.; Kooyman, P.; Masquelier, C.; Tarascon, J. M. *Chem. Mater.* **2006**, *18*, 5520−5529.
(6) Hashem, A.; Askar, M.; Winter, M.; Albering, J.; Besenhard, J. *Ionics* **2007**, *13*, 3−8.
(7) Wagemaker, M.; Borghols, W.; vanâÂĚEck, E.; Kentgens, A.; Kearley, G.; Mulder, F. *Chem.—Eur. J.* **2007**, *13*, 2023−2028.
(8) Lee, E.; Persson, K. A. *Energy Environ. Sci.* **2012**, *5*, 6047−6051.
(9) Delacourt, C.; Poizot, P.; Tarascon, J.-M.; Masquelier, C. *Nat. Mater.* **2005**, *4*, 254−260.
(10) Hong, Y.-S.; Han, C.-H.; Kim, K.; Kwon, C.-W.; Campet, G.; Choy, J.-H. *Solid State Ionics* **2001**, *139*, 75−81.
(11) Patoux, S.; Rousse, G.; Leriche, J.-B.; Masquelier, C. *Solid State Sci.* **2004**, *6*, 1113−1120.
(12) Gibot, P.; Casas-Cabanas, M.; Laffont, L.; Levasseur, S.; Carlach, P.; Hamelet, S.; Tarascon, J.-M.; Masquelier, C. *Nat. Mater.* **2008**, *7*, 741−747.
(13) Whittingham, M. S. *Chem. Rev.* **2004**, *104*, 4271−4302.
(14) Conry, T. E.; Mehta, A.; Cabana, J.; Doeff, M. M. *Chem. Mater.* **2012**, *24*, 3307−3317.
(15) Aurbach, D.; Markovsky, B.; Weissman, I.; Levi, E.; Ein-Eli, Y. *Electrochim. Acta* **1999**, *45*, 67−86.
(16) Verma, P.; Maire, P.; Novák, P. *Electrochim. Acta* **2010**, *55*, 6332−6341.
(17) Ma, X.; Kang, B.; Ceder, G. *J. Electrochem. Soc.* **2010**, *157*, A925−A931.
(18) Kim, J.-H.; Myung, S.-T.; Yoon, C. S.; Kang, S. G.; Sun, Y.-K. *Chem. Mater.* **2004**, *16*, 906.
(19) Xia, H.; Meng, Y. S.; Lu, L.; Ceder, G. *J. Electrochem. Soc.* **2007**, *154*, A737.
(20) Xiao, J.; Chen, X.; Sushko, P. V.; Sushko, M. L.; Kovarik, L.; Feng, J.; Deng, Z.; Zheng, J.; Graff, G. L.; Nie, Z.; Choi, D.; Liu, J.; Zhang, J.-G.; Whittingham, M. S. *Adv. Mater.* **2012**, *24*, 2109−2116.
(21) Pasero, D.; Reeves, N.; Pralong, V.; West, A. R. *J. Electrochem. Soc.* **2008**, *155*, A282.
(22) Kunduraci, M.; Amatucci, G. *Electrochim. Acta* **2008**, *53*, 4193−4199.
(23) Kunduraci, M.; Al-Sharab, J. F.; Amatucci, G. G. *Chem. Mater.* **2006**, *18*, 3585.
(24) Cabana, J.; Casas-Cabanas, M.; Omenya, F. O.; Chernova, N. A.; Zeng, D.; Whittingham, M. S.; Grey, C. P. *Chem. Mater.* **2012**, *24*, 2952−2964.
(25) Lee, E.-S.; Nam, K.-W.; Hu, E.; Manthiram, A. *Chem. Mater.* **2012**, *24*, 3610−3620.
(26) Chemelewski, K. R.; Shin, D. W.; Li, W.; Manthiram, A. *J. Mater. Chem. A* **2013**, *1*, 3347−3354.
(27) Janga, M.-W.; Junga, H.-G.; Scrosatia, B.; Sun, Y.-K. *J. Power Sources* **2012**, *220*, 354.
(28) Hinuma, Y.; Meng, Y. S.; Ceder, G. *Phys. Rev. B* **2008**, *77*, 224111.
(29) van de Walle, A.; Asta, M. *Modell. Simul. Mater. Sci. Eng.* **2002**, *10*, 521.
(30) Wang, L.; Li, H.; Huang, X.; Baudrin, E. *Solid State Ionics* **2011**, *193*, 32−38.
(31) Hai, B.; Shukla, A. K.; Duncan, H.; Chen, G. *J. Mater. Chem. A* **2013**, *1*, 759−769.
(32) Yi, T.-F.; Zhu, Y.-R.; Zhu, R.-S. *Solid State Ionics* **2008**, *179*, 2132−2136.
(33) Kang, B.; Ceder, G. *Nature* **2009**, *458*, 190−193.
(34) Yamazaki, Y.; Hernandez-Sanchez, R.; Haile, S. M. *J. Mater. Chem.* **2010**, *20*, 8158−8166.